Zhu, Luoyan; Liu, Yinsheng; He, Danping; Vorobyov, Sergiy A.; Zhong, Zhangdui

A Low-complexity Noise Reduction Scheme for Target Detection in the 2D Integrated Sensing And Communication System

Published in:
2023 IEEE International Conference on Communications Workshops

DOI:
10.1109/ICCWorkshops57953.2023.10283759

Published: 01/01/2023

Document Version
Peer-reviewed accepted author manuscript, also known as Final accepted manuscript or Post-print

Please cite the original version:
Zhu, L., Liu, Y., He, D., Vorobyov, S. A., & Zhong, Z. (2023). A Low-complexity Noise Reduction Scheme for Target Detection in the 2D Integrated Sensing And Communication System. In *2023 IEEE International Conference on Communications Workshops: Sustainable Communications for Renaissance, ICC Workshops 2023* (pp. 909-914). (IEEE International Conference on Communications Workshops). IEEE. https://doi.org/10.1109/ICCWorkshops57953.2023.10283759

A Low-complexity Noise Reduction Scheme for Target Detection in the Integrated MIMO Sensing And Communication System

Luoyan Zhu[†,♭], Yinsheng Liu[†,♯], Danping He[†,♯], Sergiy A. Vorobyov[♭], Zhangdui Zhong[†,♯]
[†]State Key Laboratory of Rail Traffic Control and Safety, Beijing Jiaotong University, Beijing, China 100044
[♯]Collaborative Innovation Center of Railway Traffic Safety
[♭]Department of Signal Processing and Acoustics, Aalto University, Finland
E-mail: luoyanzhu@bjtu.edu.cn, ys.liu@bjtu.edu.cn, danpinghe@bjtu.edu.cn, zhdzhong@bjtu.edu.cn, sergiy.vorobyov@aalto.fi

***Abstract*—This paper deals with low-complexity noise reduction in the multiple input multiple output integrated sensing and communication system. The conventional low-rank filter that reduces the noise significantly becomes impractical for two-dimensional (2D) arrays because of the huge computational burden caused by the 2D eigen value decomposition (EVD). To address the computational issue, first a low-complexity filter with two separated one-dimensional low-rank filters is proposed first so that the high-complexity EVD can be avoided. Furthermore, a discrete cosine transform-based filter is proposed to achieve an efficient and asymptotically equivalent denoising performance without the need for accurate estimations of sample covariance matrix. The simulation results illustrate that: i) our scheme improves the denoising performance with a low complexity and it is practically feasible; ii) decreasing the rank leads to a higher output signal to noise ratio of the target, which further results in a better detection probability.**

***Index Terms*—Noise reduction, target detection, millimeter wave (mmWave), integrated sensing and communication (ISAC)**

I. Introduction

The plethora of connected devices and services emerging in 5G-Advanced and 6G communications have motivated significant research interests in synergistic design of high-quality wireless communication systems with highly accurate and robust sensing capabilities [1], [2]. The integration of the two functions in a single system is typically referred to as integrated sensing and communication (ISAC) system [3], [4]. The motivation for such systems is mostly driven by the fact that wireless media has a limited amount of spectrum, whereas communications and remote sensing systems perform efficiently when using a larger spectrum. ISAC system has advantages of improving the spectral and energy efficiencies and minimizing hardware and signaling cost.

To achieve the sensing and communications functions simultaneously, the sensing and communication operations are jointly optimized in the same hardware platform using a unified signal processing framework [5]. While communication focuses on transmitting information via specifically designed signals and subsequently recovering it, sensing concentrates on collecting and extracting information from noisy observations. Exploiting all potential benefits of an ISAC system requires the use of adequate signal processing techniques to recover the echoes generated by multiple targets.

Joint sensing-communication waveform design criteria that would optimally balance the functionalities of sensing and communications pose major challenges [6]. ISAC frameworks were considered for single-antenna systems in [7], where typical communication and radar waveforms were optimized also for improving sensing performance. Furthermore, a loss function in [8] that captures radar performance while maintaining signal-to-interference plus noise ratio bounding guarantee was used in a multiple input multiple output (MIMO) ISAC system. It is natural for the forthcoming system to connect both millimeter wave (mmWave) ISAC systems and large antenna arrays with MIMO signal processing techniques [9]. While the linear frequency modulated continuous-wave (FMCW) signal is commonly adopted in current state-of-the-art applications to ensure a high-resolution target estimation [10], [11], it suffers from the low transmitted power resulting in weak target echoes buried in heavy background noise. Fortunately, the situation of poor signal-to-noise ratio (SNR) can be significantly improved by noise reduction methods.

In this paper, a versatile and universal target signal enhancement scheme is constructed to remove undesirable components from received signal. Meanwhile, we aim to reduce the computational burden for an ISAC system in order to guarantee SNR requirements. Particularly, the conventional two-dimensional (2D) low-rank filter has a high computation cost. Moreover, estimation of the sample covariance matrix (SCM) of a signal vector is required to employ eigen-value decomposition (EVD). The implementation requires estimation of correlation matrix of input vector, diagonalization of this matrix, and construction of required basis vectors. The required computations make such filter impractical for real-time applications. To deal

This work is supported by the Fundamental Research Funds for the Central Universities 2022JBXT001, State Key Laboratory of Rail Traffic Control and Safety (Contract: No.RCS2022ZT015), NSFC under Grant 62271043, and Beijing Natural Science Foundation L221009.

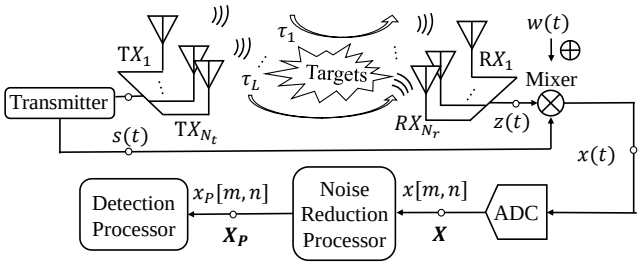

Fig. 1. Block diagram of signal processing in a MIMO ISAC system.

with this problem, the 2D low-rank filter is replaced by two separated one-dimensional (1D) low-rank filters so that the high-complexity EVD can be avoided. Moreover, whereas the EVD is signal dependent, the discrete cosine transform (DCT) is signal independent and can therefore be implemented in a computationally efficient manner, which we also exploit in our design. Simulation results illustrate that our low-complexity algorithm can significantly improve denoising performance and detection probability.

II. System Model

Wireless infrastructures and devices can also perform sensing via radio transmission and signal processing with multiple antenna arrays [12]. Thus, in this section, we consider a monostatic MIMO antenna array with N_t collocated transmit and N_r collocated receive antenna elements. Both transmit and receive antenna arrays are uniform linear arrays (ULAs), where the receive element spacings d's are half the working wavelength λ while the transmit element spacings are $d \cdot N_r$ to realize the MIMO virtual array (VA) on the transmitting side. As MIMO radars achieve waveform orthogonality by using a multiplexing technique such as time-division multiplexing (TDM), frequency-division multiplexing (FDM), and code-division multiplexing (CDM). The antenna configuration in this paper employs TDM technique for its simplicity and low-complexity in practical implementations, which can be conveniently implemented in practice for ISAC utilizations [13]. In particular, an FMCW with up- and down-chirp modulations is used for radar sensing in this work and can be flexibly leveraged for communication as well. The simplified block diagram of signal processing in a MIMO ISAC system is demonstrated in Fig. 1.

A. FMCW MIMO Signals

The transmitted signal $s(t)$ is sent from the transmitter with N_t-th antenna element (TX_{N_t}), which can be formulated using the complex representation as

$$s(t) = e^{j(2\pi f_c t + \pi \Delta f t^2) + \phi_0}, \tag{1}$$

where f_c, ϕ_0, and $\Delta f = \frac{B}{T}$ are the starting frequency, initial phase, and the chirp slope rate with B and T denoting the transmitted bandwidth and the chirp duration. Assuming L targets resulting in a superposition of L delayed versions lagged behind $s(t)$, the received signal of the n-th virtual element can be expressed as

$$z_n(t) = \sum_{l=1}^{L} \beta_l e^{j(2\pi f_c (t-\tau_{n,l}) + \pi \Delta f (t-\tau_{n,l})^2) + \phi_0}, \tag{2}$$

where β_l is the scaling amplitude backscattered from the l-th target, and $n \in [0, N-1]$ is the index with $N = N_t \cdot N_r$ denoting the number of elements in VA. The total number of virtual received antenna element from the single transmitted antenna element. After the down-conversion mixer, the intermediate frequency (IF) signal is given by

$$x_n(t) = s^*(t) z_n(t) = \sum_{l=1}^{L} \alpha_l e^{j2\pi(\Delta f \tau_{n,l} t + f_c \tau_{n,l})} + w(t), \tag{3}$$

where $\{\cdot\}^*$ represents the complex-conjugate operation. Generally, $w(t)$ is assumed to be the zero-mean stationary complex circular Gaussian noise with $\mathrm{E}\{|w(t)|^2\} = N_0$ and $\mathrm{E}\{\cdot\}$ standing for the statistical expectation. Herein, $\tau_{n,l}$ is the round trip delay in the n-th virtual antenna element, which can be given by

$$\tau_{n,l} = 2(R_l + v_l n T)/c - d(n-1)\sin(\phi_l), \tag{4}$$

with R_l, v_l, and ϕ_l denoting the distance, velocity, and the direction of departure of the l-th target, respectively. The constant α_l is the amplitude of the IF signal of the l-th target.

B. Digital Signal Model

As shown in Fig. 1, the IF signals $x_n(t)$, $n = 1, ..., N$, go to the analog-to-digital converter (ADC) for discrete sampling. Thus, they can be expressed as the $M \times N$ matrix $\boldsymbol{X}$. Denote $x[m,n]$ and $w[m,n]$ to be the discrete form of $x(t)$ and $w(t)$ at the m-th sample of the n-th virtual antenna element, that is,

$$x[m,n] \triangleq x_n(mT_s) = \sum_{l=1}^{L} \alpha_l e^{j2\pi(\frac{\theta_l}{M} m + \frac{\varphi_l}{N} n)} + w[m,n], \tag{5}$$

where T_s is the sampling interval. The Gaussian noise $w[m,n]$ corresponds here to the (m,n)-th element in the noise matrix $\boldsymbol{W}$. Moreover, θ_l and φ_l are used herein for simplicity, which consist of the parameters including τ_n, f_c, and Δf. Assuming that $\alpha_l \sim \chi^2(4)$ that corresponds to the radar cross section (RCS) fluctuation with Swerling IV model [14], and $\mathrm{E}\{\alpha_{l_1}^* \alpha_{l_2}\} = \sigma_l^2 \delta[l_1 - l_2]$ with $\delta[\cdot]$ representing the Kronecker delta function, the range-angle-correlation of $x[m,n]$ can be obtained as

$$\begin{aligned} r[\Delta m, \Delta n] &\triangleq \mathrm{E}\{x[m,n] x^*[m+\Delta m, n+\Delta n]\} \\ &= \sum_{l=1}^{L} \sigma_l^2 e^{-j2\pi(\frac{\theta_l}{M}\Delta m + \frac{\varphi_l}{N}\Delta n)} + \sigma_w^2[\Delta m, \Delta n], \end{aligned} \tag{6}$$

where $\sigma_w^2[\Delta m, \Delta n] = \mathrm{E}\{|w^*[m,n] w[m+\Delta m, n+\Delta n]|^2\}$ is the noise correlation. It has a relatively small value when

$\Delta m \neq 0$ and $\Delta n \neq 0$. Accordingly, the range-correlation of $x[m,n]$ can be found to be

$$r_R[\Delta m] \triangleq r[\Delta m, 0] = \sum_{l=1}^{L} \sigma_l^2 e^{-j2\pi \frac{\theta_l}{M}\Delta m} + \sigma_w^2[\Delta m]. \quad (7)$$

Similarly, the angle-correlation of $x[m,n]$ without considering the range-correlation, indicating $\Delta m = 0$, is independent to the range index m, that is,

$$r_D[\Delta n] \triangleq r[0, \Delta n] = \sum_{l=1}^{L} \sigma_l^2 e^{-j2\pi \frac{\varphi_l}{N}\Delta n} + \sigma_w^2[\Delta n]. \quad (8)$$

III. Proposed Noise Reduction Scheme

In this section, the proposed scheme is presented to suppress the noise power. We first introduce the conventional 2D low-rank algorithm. Then, the low-complexity DCT-based scheme is proposed stage by stage. It works in two stages to balance the computational complexity and the practical feasibility.

A. Brief Review of Conventional 2D Low-Rank Filter

Using the fact that the signal subspace spanned by the received signals is dominated by the target echoes, the 2D low-rank filter can reduce the noise significantly. The idea is to use the energy-concentrating, i.e., low-rank property of the eigen-domain [15] to reduce noise. Let $\boldsymbol{x} \in \boldsymbol{C}^{K\times 1}$ be a vector representation of the signal matrix $\boldsymbol{X}$, that is, $\boldsymbol{x} = \mathrm{vec}(\boldsymbol{X})$. Then the SCM is defined by

$$\boldsymbol{R}_{\boldsymbol{x}} \triangleq \mathrm{E}\{\boldsymbol{x}\boldsymbol{x}^{\mathrm{H}}\} \in \boldsymbol{C}^{K\times K}, \quad K = MN, \quad (9)$$

where $\{\cdot\}^{\mathrm{H}}$ is the Hermitian transpose. The EVD of $\boldsymbol{R}_{\boldsymbol{x}}$, as well as its low rank approximation, are given as

$$\boldsymbol{R}_{\boldsymbol{x}} = \boldsymbol{U}_{\boldsymbol{x}}\boldsymbol{\Lambda}_{\boldsymbol{x}}\boldsymbol{U}_{\boldsymbol{x}}^{\mathrm{H}} \approx \boldsymbol{R}_{\boldsymbol{x}_P} = \boldsymbol{U}_{\boldsymbol{x}}\boldsymbol{\Lambda}_{\boldsymbol{x}_P}\boldsymbol{U}_{\boldsymbol{x}}^{\mathrm{H}} \in \boldsymbol{C}^{K\times K}, \quad (10)$$

where $\boldsymbol{U}_{\boldsymbol{x}}$ is a unitary matrix of eigenvectors, and $\boldsymbol{\Lambda}_{\boldsymbol{x}} = \mathrm{diag}\{\lambda_x[k]\}_{k=1}^{k=K}$ is the diagonal matrix that consists of eigenvalues $\lambda_x[k]$ ordered in descending order. Accordingly, if most power can be captured in low-rank space, the EVD can be approximated by $\boldsymbol{R}_{\boldsymbol{x}_P}$ with $\boldsymbol{\Lambda}_{\boldsymbol{x}_P}$ denoting a truncated diagonal matrix with elements $\{\lambda_x[k]\}_{k=1}^{k=P}$ and $\{0\}_{k=P+1}^{k=K}$. Based on that, the 2D low-rank filter similar to [16] can be deduced from the perspective of maximum likelihood estimation (MLE), and it is given by

$$\boldsymbol{x}_P \triangleq \mathrm{vec}(\boldsymbol{X}_P) = \boldsymbol{U}_{\boldsymbol{x}}\boldsymbol{\Delta}_{\boldsymbol{x}}\boldsymbol{U}_{\boldsymbol{x}}^{\mathrm{H}}\boldsymbol{x}, \quad (11)$$

where $\boldsymbol{\Delta}_{\boldsymbol{x}}$ is given by

$$\boldsymbol{\Delta}_{\boldsymbol{x}} = \begin{pmatrix} \boldsymbol{\Delta}_{\boldsymbol{x}_P} & \boldsymbol{0} \\ \boldsymbol{0} & \boldsymbol{0} \end{pmatrix} \quad (11a)$$

with a diagonal matrix $\boldsymbol{\Delta}_{\boldsymbol{x}_P}$. Specifically, the (k,k)-th element of $\boldsymbol{\Delta}_{\boldsymbol{x}}$ is denoted by

$$[\boldsymbol{\Delta}_{\boldsymbol{x}}]_{k,k} = \begin{cases} \frac{1}{1+\lambda_x[k]^{-1}\gamma^{-1}}, & k = 1,2,\cdots,P, \\ 0, & k = P+1,\cdots,K, \end{cases} \quad (11b)$$

where γ denotes the SNR. In (11), $\boldsymbol{x}$ and $\boldsymbol{x}_P$ are taken as input and output of the filter, respectively.

However, the conventional 2D filter is computationally inconvenient in practice for the following two reasons:

i. As $\boldsymbol{R}_{\boldsymbol{x}}$ is constructed as an $MN \times MN$ matrix, its EVD has high complexity. The sharp increase of complexity is often unacceptable in practice.
ii. The estimation of $\boldsymbol{R}_{\boldsymbol{x}}$ can be obtained by (9), as long as there are enough number of samples. However, the vectorized signals $\boldsymbol{x}$ is obtained from the signal matrix $\boldsymbol{X}$, which is a single sample matrix in a single chirp measurement. Thus, we have the only one sample that leads towards an infeasible estimation of $\boldsymbol{R}_{\boldsymbol{x}}$.

To deal with the aforementioned two problems, the noise reduction scheme with a low complexity that is feasible in practice is proposed next. It works in two stages.

B. First Stage: Low-Complexity Filter

The 2D filter is accompanied by a huge computation burden as the EVD is performed over a very large size matrix. To address the issue of high computation burden, a low-complexity filter with two separated 1D low-rank filters is proposed in the first stage. Specifically, based on (6), (7), and (8) we can use the approximation

$$r[\Delta m, \Delta n] \approx r[\Delta m] \cdot r[\Delta n]. \quad (12)$$

The equation holds as an exact equality if only one target appears, that is $L = 1$. Although (12) is only an approximation when $L > 1$, we can use it to avoid the high-complexity EVD, and still see little degradation of performance ias will be shown by simulation results. Thus, the covariance matrix can be approximated by using the Kronecker product $\otimes$ as

$$\boldsymbol{R}_{\boldsymbol{x}} \approx \boldsymbol{R}_m \otimes \boldsymbol{R}_n, \quad (13)$$

where $\boldsymbol{R}_m$ and $\boldsymbol{R}_n$ are the range-correlation and angle-correlation matrices leading to the two separated 1D filters as shown in Fig. 2.

Although (11) becomes available after obtaining $\boldsymbol{R}_{\boldsymbol{x}}$ by (13), the 2D filter is still unacceptable due to the high computational burden. Therefore, the first-stage low-complexity filter aims to achieve practical feasibility by operating only with estimations of $\boldsymbol{R}_m$ and $\boldsymbol{R}_n$. The reduction of computations is achieved because of EVD and low-rank approximations of much smaller matrices $\boldsymbol{R}_m$ and $\boldsymbol{R}_n$ (similar to (10)), that is

$$\boldsymbol{R}_m \approx \boldsymbol{R}_{m_P} = \boldsymbol{U}_m\boldsymbol{\Lambda}_{m_P}\boldsymbol{U}_m^{\mathrm{H}}, \quad (14)$$

$$\boldsymbol{R}_n \approx \boldsymbol{R}_{n_P} = \boldsymbol{U}_n\boldsymbol{\Lambda}_{n_P}\boldsymbol{U}_n^{\mathrm{H}}, \quad (15)$$

where $\boldsymbol{\Lambda}_{m_P}$ and $\boldsymbol{\Lambda}_{n_P}$ are truncated diagonal matrices with $\{\lambda_m[m]\}_{m=1}^{m=P}$ and $\{0\}_{m=P+1}^{m=M}$, $\{\lambda_n[n]\}_{n=1}^{n=P}$ and $\{0\}_{n=P+1}^{n=N}$, as diagonal elements in descending order, respectively. The unitary matrices, $\boldsymbol{U}_m$ and $\boldsymbol{U}_n$ correspond to the separated transformers $\boldsymbol{C}_m$ and $\boldsymbol{C}_n$ in Fig. 2, respectively. Based on the EVD and low-rank approximations of $\boldsymbol{R}_m$ and $\boldsymbol{R}_n$ and using equation $\mathrm{vec}(\boldsymbol{ABC}) = (\boldsymbol{C}^{\mathrm{T}} \bigotimes \boldsymbol{A})\mathrm{vec}(\boldsymbol{B})$ in [17], we obtain the P-rank approximation as

$$\begin{aligned} \mathrm{vec}(\boldsymbol{X}_P) &= (\boldsymbol{U}_m \otimes \boldsymbol{U}_n)\boldsymbol{\Delta}_{\boldsymbol{x}}(\boldsymbol{U}_m \otimes \boldsymbol{U}_n)^{\mathrm{H}}\mathrm{vec}(\boldsymbol{X}) \\ &= \mathrm{vec}\{\boldsymbol{U}_n[\boldsymbol{\Delta} \odot (\boldsymbol{U}_n^{\mathrm{H}}\boldsymbol{X}\boldsymbol{U}_m^{*})]\boldsymbol{U}_m^{\mathrm{T}}\}. \end{aligned} \quad (16)$$

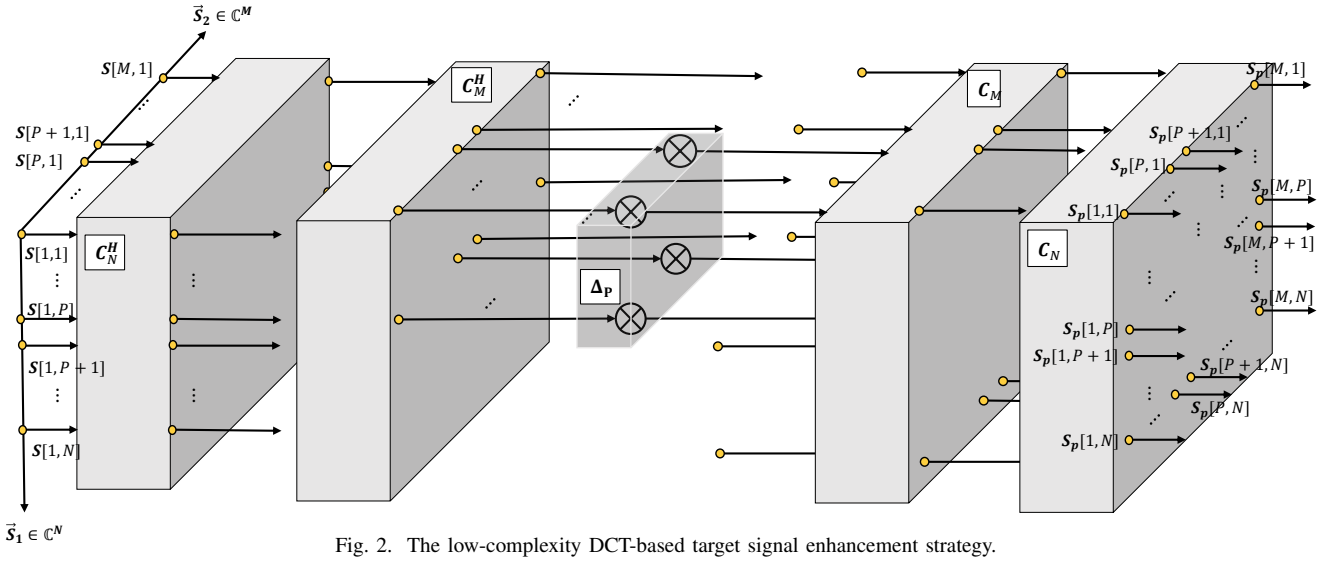

Fig. 2. The low-complexity DCT-based target signal enhancement strategy.

Herein, $\boldsymbol{\Delta}$ is a truncated matrix given by

$$\boldsymbol{\Delta} = \begin{pmatrix} \boldsymbol{\Delta}_P & \mathbf{0} \\ \mathbf{0} & \mathbf{0} \end{pmatrix}, \tag{16a}$$

where the (m,n)-th element in $\boldsymbol{\Delta}_P$ is given by

$$[\boldsymbol{\Delta}_P]_{m,n} = \begin{cases} \frac{1}{1+\lambda_m^{-1}[m]\lambda_n^{-1}[n]}, & \text{if } m \le P, n \le P, \\ 0, & \text{otherwise.} \end{cases} \tag{16b}$$

C. Second Stage: DCT-Based Filter

So far, the EVD in the low-complexity filter is performed for estimating SCM. Noted that the ideal estimations of $\boldsymbol{R}_{\boldsymbol{x}}$, $\boldsymbol{R}_m$ and $\boldsymbol{R}_n$ rely on sufficiently many samples, which is hardly achieved in practice. Fortunately, for a stationary zero-mean, first-order Markov process, DCT provides a predetermined set of basis vectors that, together, give a good approximation [18]. By exploiting this property, the DCT based filter is used in the second stage to develop an efficient noise reduction algorithm. Particularly, whereas EVD is a signal-dependent transformation, the DCT is signal independent and can therefore be implemented in a computationally efficient manner for FMCW signals.

Specifically, the factors $\boldsymbol{U}_m$, $\boldsymbol{U}_n$, and $\boldsymbol{\Delta}$ can be substituted and derived from DCT, which are formerly employed to make the low-complexity filter in (16). Denote the DCT of the signal vectors in the signal matrix $\boldsymbol{X}$ as

$$\boldsymbol{c}_m(n) = k_m \sum_{i=1}^{N} x[m,n] \cos\left(\frac{(2i+1)\pi}{2N} n\right), \tag{17}$$

with the constant k_m given by

$$k_m = \begin{cases} \sqrt{\frac{1}{N}}, & n = 1, \\ \sqrt{\frac{2}{N}}, & n \neq 1. \end{cases} \tag{18}$$

For convenience of presentation, we rewrite (17) as

$$\boldsymbol{c}_m = \mathcal{DCT}\{\boldsymbol{x}_m\} \triangleq \boldsymbol{C}_m \boldsymbol{x}_m, \tag{19}$$

where $\boldsymbol{x}_m$ is the m-th row in the signal matrix $\boldsymbol{X}$ and $\boldsymbol{C}_m$ is the transformation matrix of DCT making the approximation of $\boldsymbol{C}_m \approx \boldsymbol{U}_m$. Accordingly, we have $\boldsymbol{C}_n \approx \boldsymbol{U}_n$ because the DCT matrix of the n-th column in the signal matrix $\boldsymbol{X}$ can be given by

$$\boldsymbol{c}_n = \mathcal{DCT}\{\boldsymbol{x}_n\} = \boldsymbol{C}_n \boldsymbol{x}_n, \tag{20}$$

where

$$\boldsymbol{c}_n(m) = k_n \sum_{i=1}^{M} x[m,n] \cos\left(\frac{(2i+1)\pi}{2M} m\right). \tag{21}$$

The only issue that remains to be considered in the design of the DCT-based low-complexity algorithm is how to estimate the eigenvalues of $\boldsymbol{\Delta}$. Assuming that the stochastic processes responsible for generating the input vectors $\boldsymbol{x}_m$ and $\boldsymbol{x}_n$ are ergodic, we may obtain an estimate of its correlation matrices $\widehat{\boldsymbol{R}}_m$ and $\widehat{\boldsymbol{R}}_n$. Herein, we take $\widehat{\boldsymbol{R}}_m$ to exemplify the derivation without the estimation of $\boldsymbol{R}_m$, which is given by

$$\widehat{\boldsymbol{R}}_m = \frac{1}{M} \sum_{m=1}^{M} \boldsymbol{x}_m \boldsymbol{x}_m^{\mathrm{T}}, \tag{22}$$

Then, considering (19) associated with the eigenvectors $\boldsymbol{U}_m$ of $\widehat{\boldsymbol{R}}_m$, the approximation may be written in the form

$$\lambda_m[m] \approx \boldsymbol{C}_m \widehat{\boldsymbol{R}}_m \boldsymbol{C}_m^{\mathrm{T}} = \frac{1}{M} \sum_{m=1}^{M} \boldsymbol{c}_m \boldsymbol{c}_m^{\mathrm{T}}. \tag{23}$$

Similarly, λ_n is given by

$$\lambda_n[n] \approx \boldsymbol{C}_n \widehat{\boldsymbol{R}}_n \boldsymbol{C}_n^{\mathrm{T}} = \frac{1}{N} \sum_{n=1}^{N} \boldsymbol{c}_n \boldsymbol{c}_n^{\mathrm{T}}. \tag{24}$$

More specifically, the eigenvalue spread is equal $(1+\rho)$ after DCT and power normalization, where $\rho \in [0,1]$ is the adjacent correlation coefficient of the input signals [19]. This can be used in the case when the correlations between various input signals are defined with ρ.

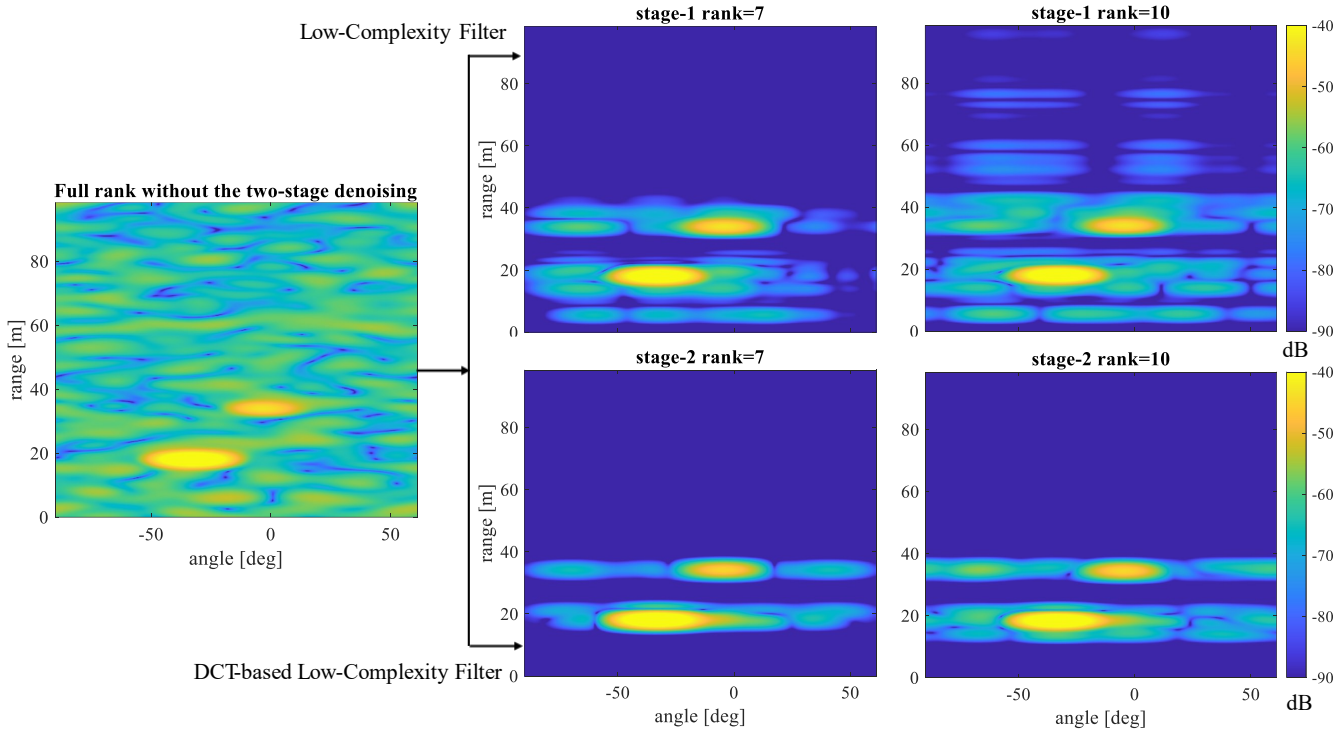

Fig. 3. Performance comparisons of 2D low-complexity scheme under different rank selections for the two stages. The value of the colorbar is uniform for different subfigures.

TABLE I
SYSTEM PARAMETERS

Parameter	Value	Parameter	Value
Center Frequency (f_c [GHz])	77	Samples/Chirp (M)	256
Sampling Rate ($\frac{1}{T_s}$ [MS/s])	6.3	Virtual elements (N)	16
Chirp Slope (Δf [MHz/μs])	85.17	Bandwidth (B [GHz])	2.51

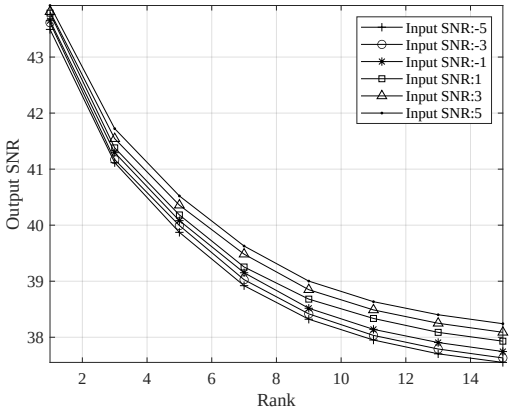

Fig. 4. The output SNR against the rank.

IV. SIMULATION RESULTS

In this section, we provide some numerical results to illustrate the advantages of the proposed low-complexity DCT-based filter. Computer simulations with the configuration shown in Table I are performed. We consider an ISAC system under the time-division multiplexing (TDM)-MIMO configuration with $N_t = 2$ transmit and $N_r = 8$ receive antenna elements utilizing Monte Carlo trials to investigate the denoising performance. The effect of rank variation is mainly evaluated by 100 independent trials with two-target appearance.

For the sake of exhibiting the advantages of the two stages of the proposed algorithm, we illustrate and compare the denoising performance by conducting the two filters separately as shown in Fig. 3. Herein, the analysis focuses on two-target appearances at the range-angles of (38 m, 2 deg) and (21 m, -45 deg). For the condition of full rank suggesting no denoising, the noise is observed the most. It is then used as a benchmark for comparison. Different selections of rank lead to different target power and noise levels in both stages. In the stage-1 of low-complexity filter, the noise level can be well suppressed under the condition of $rank = 7$ and $rank = 10$, where the computation burden is reduced with the two separate 1D EVD filters. In the second stage, one step forward from stage-1, DCT is adopted to avoid the estimation of SCM. We can see that stage-2 performs even better than stage-1 as the noise level around the target is relatively weak.

Fig. 4 shows the significant decrease of the output SNR of the target along with the increased rank. The analysis focuses on the first one of the two targets which appearances at the range-angle of (38 m, 2 deg). Simulations under different input SNRs of the target, (which are the SNR values before implementing the noise reduction scheme) are performed here. Herein, the rank shown in the figure denotes the angle-dimension, while the rank in the range-dimension is selected by maintaining the same proportion between the selected

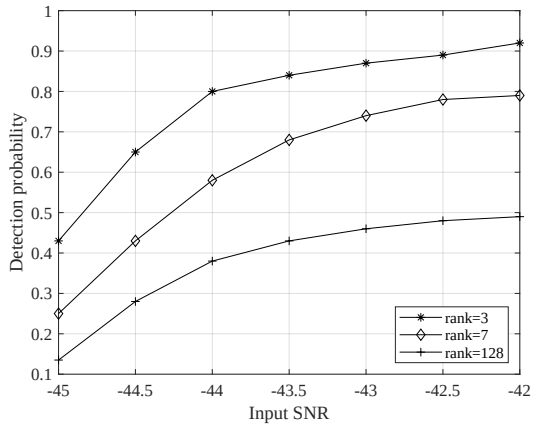

Fig. 5. The detection probability against target input SNR variation.

rank and the dimension. The main insight of this figure is the significant reduction of the output SNR along with the increasing rank. In addition, when the full rank is selected, the output SNRs of four plots are still higher than the input SNRs. This is mainly because the output SNR is improved not only by the proposed filter, but also thanks to the coherent superposition gain from DFT. Fig. 5 illustrates the noise reduction of the proposed scheme from the perspective of detection enhancement. The Cell Average-Constant False Alarm Rate (CA-CFAR) detector is applied here with a constant false alarm probability P_{fa} of 10^{-14}. Three selections of ranks are chosen to illustrate the detection performance under different conditions. The CA-CFAR detector carries out a judgement by comparing the power of the cell under test (CUT) to an adaptive threshold calculated from the average power of the training cells (TC). In other words, the larger power gap between the CUT and average of TC, the more likely CUT power exceeds its threshold, indicating a target here. The detection probability P_d increases significantly as the rank decreases to generate a larger power gap by filtering the noise power in training cells of the detector. The three plots show that the detection performance is improved as the input SNR increases. Besides, the improvement can be signified by the reduced rank, as the detection probability P_d increases when the rank gets smaller. This is aligned with the results in Fig. 4 as the detection probability depends mostly on the SNR of the target. Hence, a smaller $rank$ indicates a more significant performance improvement of noise reduction.

V. Conclusion

In this paper, we have proposed a two-stage low-complexity target signal enhancement scheme using FMCW signals. The conventional 2D low-rank filter that reduces noise significantly has a high computation cost because of 2D EVD. Thus, here, the 2D low-rank filter has been replaced by two separated 1D low-rank filters so that the high-complexity EVD can be avoided. Moreover, whereas the EVD is signal dependent, the DCT is signal independent and has been therefore implemented to also avoid estimation of the SCM. Simulation results have illustrated that our scheme improves the denoising performance with a low complexity. In addition, decreasing the rank leads to a higher output SNR of the target, which further results in a better detection probability. The results have illustrated that the proposed scheme can be implemented in a computationally efficient manner and be practical for real-time applications.

References

[1] G. Cheng and J. Xu, "Coordinated transmit beamforming for multi-antenna network integrated sensing and communication," *arXiv preprint arXiv:2211.01085*, 2022.

[2] J. A. Zhang, F. Liu, C. Masouros, R. W. Heath, Z. Feng, L. Zheng, and A. Petropulu, "An overview of signal processing techniques for joint communication and radar sensing," *IEEE Journal of Selected Topics in Signal Processing*, vol. 15, no. 6, pp. 1295–1315, 2021.

[3] F. Liu, Y. Cui, C. Masouros, J. Xu, T. X. Han, Y. C. Eldar, and S. Buzzi, "Integrated sensing and communications: Toward dual-functional wireless networks for 6G and beyond," *IEEE Journal on Selected Areas in Communications*, vol. 40, no. 6, pp. 1728–1767, 2022.

[4] F. Dong, F. Liu, Y. Cui, W. Wang, K. Han, and Z. Wang, "Sensing as a service in 6G perceptive networks: A unified framework for ISAC resource allocation," *IEEE Transactions on Wireless Communications*, pp. 1–1, 2022.

[5] C. Pan, R. Zhang, M. Di Renzo, A. L. Swindlehurst, and Y.-J. A. Zhang, "Editorial introduction to the issue on advanced signal processing for reconfigurable intelligent surface-aided 6G networks," *IEEE Journal of Selected Topics in Signal Processing*, vol. 16, no. 5, pp. 880–882, 2022.

[6] P. Kumari, S. A. Vorobyov, and R. W. Heath, "Adaptive virtual waveform design for millimeter-wave joint communication-radar," *IEEE Transactions on Signal Processing*, vol. 68, pp. 715–730, 2020.

[7] S. D. Liyanaarachchi, T. Riihonen, C. B. Barneto, and M. Valkama, "Optimized waveforms for 5G–6G communication with sensing: Theory, simulations and experiments," *IEEE Transactions on Wireless Communications*, vol. 20, no. 12, pp. 8301–8315, 2021.

[8] X. Liu, T. Huang, N. Shlezinger, Y. Liu, J. Zhou, and Y. C. Eldar, "Joint transmit beamforming for multiuser MIMO communications and MIMO radar," *IEEE Transactions on Signal Processing*, vol. 68, pp. 3929–3944, 2020.

[9] H. Zheng, Z. Shi, C. Zhou, M. Haardt, and J. Chen, "Coupled coarray tensor CPD for DOA estimation with coprime l-shaped array," *IEEE Signal Processing Letters*, vol. 28, pp. 1545–1549, 2021.

[10] S. Sun, A. P. Petropulu, and H. V. Poor, "MIMO radar for advanced driver-assistance systems and autonomous driving: Advantages and challenges," *IEEE Signal Processing Magazine*, vol. 37, no. 4, pp. 98–117, 2020.

[11] F. Engels, P. Heidenreich, A. M. Zoubir, F. K. Jondral, and M. Wintermantel, "Advances in automotive radar: A framework on computationally efficient high-resolution frequency estimation," *IEEE Signal Processing Magazine*, vol. 34, no. 2, pp. 36–46, 2017.

[12] Y. Cui, F. Liu, X. Jing, and J. Mu, "Integrating sensing and communications for ubiquitous iot: Applications, trends, and challenges," *IEEE Network*, vol. 35, no. 5, pp. 158–167, 2021.

[13] K. Rambach and B. Yang, "MIMO radar: Time division multiplexing vs. code division multiplexing," in *International Conference on Radar Systems (Radar 2017)*, 2017, pp. 1–5.

[14] P. Swerling, "Probability of detection for fluctuating targets," *IRE Transactions on Information theory*, vol. 6, no. 2, pp. 269–308, 1960.

[15] C. Maccone, *Mathematical SETI: statistics, signal processing, space missions*. Springer Science & Business Media, 2012.

[16] O. Edfors, M. Sandell, J.-J. van de Beek, S. Wilson, and P. Borjesson, "OFDM channel estimation by singular value decomposition," *IEEE Transactions on Communications*, vol. 46, no. 7, pp. 931–939, 1998.

[17] X. Zhang, *Matrix analysis and applications*. Cambridge University Press, 2017.

[18] U. Grenander and G. Szegö, *Toeplitz forms and their applications*. Univ of California Press, 1958.

[19] F. Beaufays, "Transform-domain adaptive filters: An analytical approach," *IEEE Transactions on Signal processing*, vol. 43, no. 2, pp. 422–431, 1995.